Increase in Ce^{3+} Concentration of Ceria Nanoparticles for High Removal Rate of SiO_2 in Chemical Mechanical Planarization

ECS Journal of Solid State Science and Technology, **6** (9) P681-P685 (2017)
2162-8769/2017/6(9)/P681/5/$37.00 © The Electrochemical Society

Increase in Ce^{3+} Concentration of Ceria Nanoparticles for High Removal Rate of SiO_2 in Chemical Mechanical Planarization

Kijung Kim,[a] Dong Kee Yi,[b,z] and Ungyu Paik[a,c,z]

[a]*Department of Nanoscale Semiconductor Engineering, Hanyang University, Seoul 04763, South Korea*
[b]*Department of Chemistry, Myongji University, Yongin 18448, South Korea*
[c]*Department of Energy Engineering, Hanyang University, Seoul 04763, South Korea*

Ceria nanoparticles (NPs) are used as abrasives for silicon dioxide (SiO_2) chemical mechanical planarization (CMP) due to the strong chemical bonds between the Ce^{3+} ions of ceria NPs and the hydrated silicate species on the surface of SiO_2 films. However, the limited concentration of Ce^{3+} ions in ceria NPs remains a major challenge for this application. Herein, we report a simple strategy to synthesize ceria NPs with high concentrations of Ce^{3+} ions for enhanced adsorption reactions with silicate anions. Three types of ceria NPs approximately 70 nm in size were synthesized via the aggregation of different sized primary NPs. As the particle size of the primary NPs decreased from 70 nm to 5 nm, the Ce^{3+} concentration of the ceria NPs increased from 15.6 to 24.0%. The adsorption isotherm fits the Freundlich model and the constants of adsorption capacity (K_F) and adsorption intensity (1/n) indicate that the adsorption affinity for silicate anions increased with increasing Ce^{3+} concentration. The increase in Ce^{3+} concentration led to an increase in the chemical adsorption between ceria NPs and silicate anions, resulting in a high removal rate of SiO_2 during CMP.
 [DOI: 10.1149/2.0371709jss]

Manuscript submitted July 14, 2017; revised manuscript received August 22, 2017. Published September 20, 2017.

Ceria nanoparticles (NPs) have been used as promising materials in various applications such as wastewater treatment, solid oxide fuel cells, and chemical mechanical planarization (CMP).[1–6] In many of these applications, the high performance of ceria NPs is attributed to their strong ability to take-up and release oxygen, resulting in a change in the oxidation state of cerium ions from Ce^{3+} to Ce^{4+}. Ce^{3+} ions are considered to be the reactive sites on the surfaces of ceria NPs.[7–10] In CMP applications, the Ce^{3+} ions on the surface of ceria NPs react with hydrated silicate species on the surface of silicon dioxide (SiO_2) films, resulting in the formation of strong Ce-O-Si bonds that can improve the polishing efficiency of SiO_2.[7,11] However, the low Ce^{3+} concentrations in ceria NPs remain a major challenge for CMP applications.

Many approaches have been studied to increase in the concentration of Ce^{3+} ions in ceria NPs, such as the introduction of dopants and reducing the particle size.[12–14] Among these, decreasing the particle size is the most powerful technique to increase Ce^{3+} concentration compared to other approaches.[14–16] As particle size decreases, the loss of oxygen on the surface of ceria NPs leads to a high lattice strain, resulting in an increase in the Ce^{3+} concentration.[15,16] The concentration of Ce^{3+} ions is remarkably increased when the particle size decreased below 10 nm.[17] However, in CMP applications, the use of small particles below 10 nm leads to a decrease in the polishing efficiency of SiO_2.[18] Therefore, it is desirable to develop a new approach to increase in the Ce^{3+} concentration of ceria NPs as abrasives for SiO_2 CMP.

Herein, we report a new strategy to resolve the limited Ce^{3+} concentration in ceria NPs, and we investigate the role of Ce^{3+} concentration in ceria NPs for silicate adsorption for high SiO_2 film removal rates. In our approach, the particle size reduction method was adopted to increase the concentration of Ce^{3+} ions. However, the average particle size was controlled in the range of 60 to 80 nm by aggregation of the ceria primary NPs. Three different types of ceria NPs (small, medium, and large ceria NPs, hereafter noted as S-ceria, M-ceria, and L-ceria NPs, respectively) were composed of approximately 5, 20, and 70 nm sized primary ceria NPs as building units, respectively. As the size of the primary ceria NPs decreased, the Ce^{3+} concentration increased. The adsorption isotherms of silicate anions with the S-ceria, M-ceria, and L-ceria NPs were acquired and were fitted by using both the Langmuir and Freundlich models. We applied all the ceria NPs as abrasives for the CMP of SiO_2 films. The removal rate of SiO_2 increased with the increased silicate adsorption observed in adsorption isotherm analysis.

Experimental

Materials.—Cerium nitrate hexahydrate ($Ce(NO_3)_3 \cdot 6H_2O$, Sigma Aldrich, St. Louis, Missouri, US) was used as a precursor to synthesize the ceria NPs. Poly(vinyl pyrrolidone) (PVP K30, Sigma Aldrich, St. Louis, Missouri, US) and urea ($CO(NH_2)_2$, Sigma Aldrich, St. Louis, Missouri, US) were used to support the synthesis of ceria NPs. Sodium metasilicate ($Na_2SiO_3 \cdot 9H_2O$, Sigma Aldrich, St. Louis, Missouri, US) was used to acquire silicate adsorption isotherms with ceria NPs. Ammonium hydroxide (NH_4OH, 28–30 wt%, Junsei Chemical, Tokyo, Japan) and nitric acid (HNO_3, 1.0 N, Sigma Aldrich, St. Louis, Missouri, US) were used to adjust the pH. Blanket SiO_2 films were deposited on 200 mm diameter silicon wafers by means of plasma enhanced oxide deposition from tetraethyl orthosilicate. The thickness of the as-deposited SiO_2 films was found to be 6000 Å. A 200 mm diameter wafer was cut into several 6 × 6 cm^2 pieces for polishing experiments.

Synthesis of ceria NPs.—The strategy to synthesize S-ceria, M-ceria, and L-ceria NPs is schematically shown in Figure 1. PVP (1.08 g) and urea (0.24 g) were added to a 0.6 g solution of $Ce(NO_3)_3$ in deionized water (114 g) under vigorous stirring. To control of the particle size of the ceria primary NPs, the concentration of $Ce(NO_3)_3$ was 0.6, 3.0, and 9.0 g for S-ceria, M-ceria, and L-ceria, respectively. Subsequently, H_2O_2 (1.2 g) was added to the solution, and then the mixture was stirred for 1 h. The solution was then transferred to a

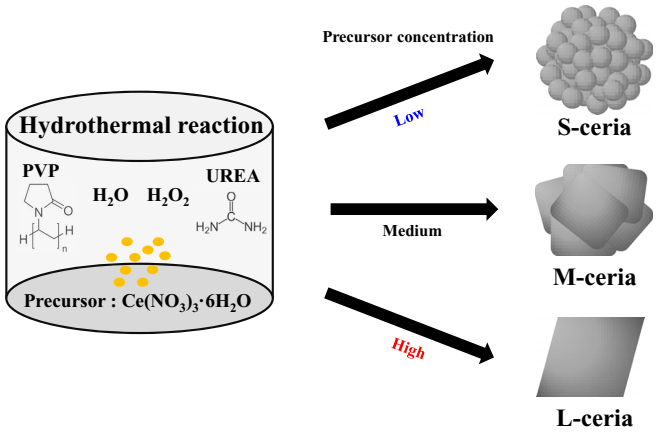

Figure 1. Schematic illustration of the formation of S-ceria, M-ceria, and L-ceria NPs.

[z]E-mail: upaik@hanyang.ac.kr; vitalis@mju.ac.kr

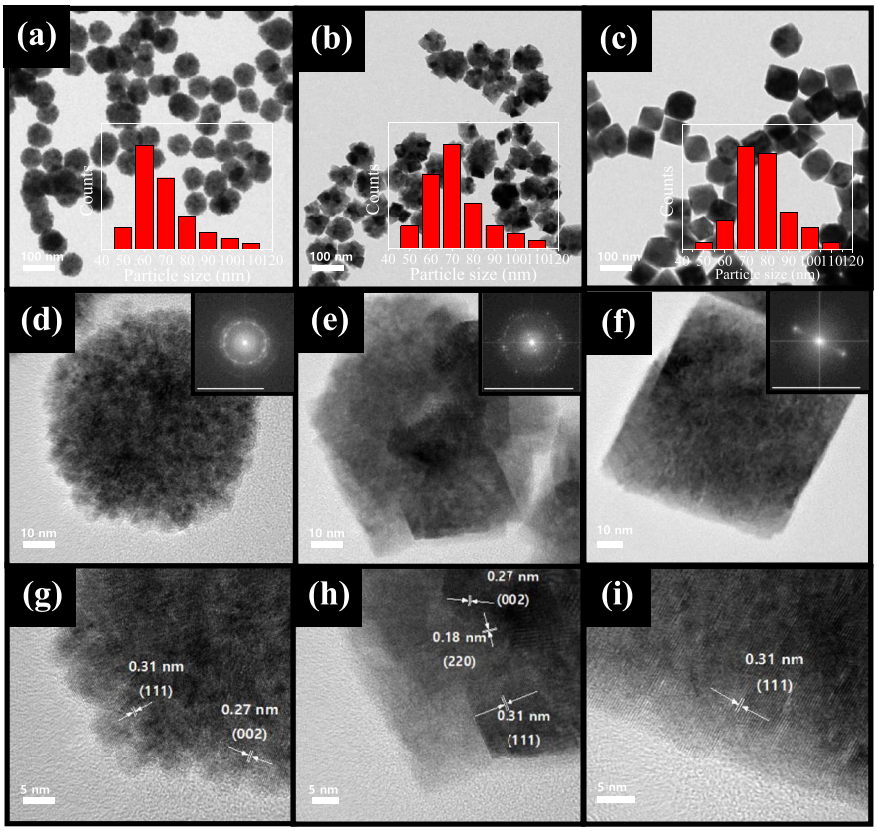

Figure 2. TEM images of (a, d, g) S-ceria, (b, e, h) M-ceria, and (c, f, i) L-ceria NPs. The insets in (a, b, c) are particle size distributions. The insets in (d, e, f) are FFT patterns.

Teflon bottle and was placed in a stainless steel autoclave at 180°C for 10 h. The sample was then centrifugally washed with water 3 times and then dried at 80°C for 24 h. After that, the sample was calcined at 500°C for 2 h to remove the remaining PVP and urea. In our synthesis process, the formation mechanism of spherical shaped ceria NPs is proposed as follows: (i) primary ceria NPs synthesized by the reactions between urea and cerium precursor in hydrothermal solutions; (ii) these primary ceria NPs are aggregated into bigger crystallites to reduce their surface energy in the following hydrothermal reaction because the small ceria NPs have high surface energy. In these processes, PVP assists the oriented aggregation of primary ceria NPs, resulting in the spherical shaped ceria NPs. In addition, the particle size of primary ceria NPs is controlled by the change of the concentration of cerium precursor.

Characterization.—The detailed structural features of S-ceria, M-ceria, and L-ceria NPs were investigated by means of high-resolution transmission electron microscopy (HR-TEM, JEM-2100F, JEOL, Tokyo, Japan). The particle size distribution of all the ceria NPs were calculated from the TEM images using the Image-J analysis software. The hydrodynamic diameters of all the ceria NPs were measured using dynamic light scattering (DLS) method (Nano-ZS, Malvern Instruments, Worcestershire, UK). X-ray diffraction patterns of S-ceria, M-ceria, and L-ceria NPs were estimated using a high-resolution X-ray diffraction analyzer (HR-XRD, Smartlab, Rigaku, Tokyo, Japan). The concentration of Ce^{3+} ions was calculated by means of X-ray photoelectron spectroscopy (XPS, Thermo fisher scientific, Waltham, Massachusetts, US). The nanotopography of SiO_2 and Si_3N_4 film was measured with a commercial multimode atomic force microscope (AFM, XE-150, Park System, Suwon, Korea). The Si AFM tip (SI-CONGG, AppNano, Mountain View, US) was used to investigate the surface roughness using non-contact mode.

Adsorption isotherm analysis.—Adsorption isotherms were plotted by using data from inductively coupled plasma atomic emission spectroscopy (ICP-OES, Optima 8300, Perkin-Elmer, Waltham, Massachusetts, USA). Ceria NP suspension samples were prepared having various concentrations of silicate anions; the pH of each suspension was adjusted to 7. The mixtures were equilibrated for 12 h, during which time they were continuously agitated by means of rolling. The suspensions were then centrifuged to remove the ceria and the adsorbed silicate anions. The supernatants were further clarified by using 0.02 μm syringe filters (Anotop 25, Whatman plc, Maidstone, kent, UK). They were then analyzed in triplicate by means of ICP. Results were corrected for ICP background by using a blank solution derived from a native ceria suspension in the absence of silicate anions. ICP responses were converted to masses via an experimentally determined calibration curve. Adsorption isotherms were calculated by determining the difference between the added silicate amounts and the amounts remaining in the supernatants.

CMP evaluations.—S-ceria, M-ceria, and L-ceria NPs were used as abrasives for SiO_2 CMP as 1.0 wt% dispersions in deionized water. The pH of all slurries was adjusted to pH 7. CMP was performed by using coupon CMP tools (CP-4, CETR, Billerica, Massachusetts, US) with an industrial standard CMP pad (IC 1010/ Suba IV, Dow Chemical, Philadelphia, Pennsylvania, US). Table S1 lists the CMP conditions used. After CMP, cleaning of the SiO_2 wafer was carried out using a standard cleaning 1 (SC 1) solution, which was composed of NH_4OH, H_2O_2, and H_2O. The thickness of the SiO_2 film was measured by using a UVISEL spectroscopic ellipsometer (MM-16, Jobin Yvon Horiba, Kyoto, Japan).

Results and Discussion

We synthesized three types of ceria NPs (S-ceria, M-ceria, and L-ceria NPs) with similar particle size distributions. Although the particle size distributions of all the ceria NPs were similar, the particle sizes of ceria primary NPs used as building units were different for the different Ce^{3+} concentrations of ceria NPs. Figure 2 shows the TEM images of S-ceria, M-ceria, and L-ceria NPs. TEM analyses of all the ceria NPs showed that their particle sizes ranged from 50 to

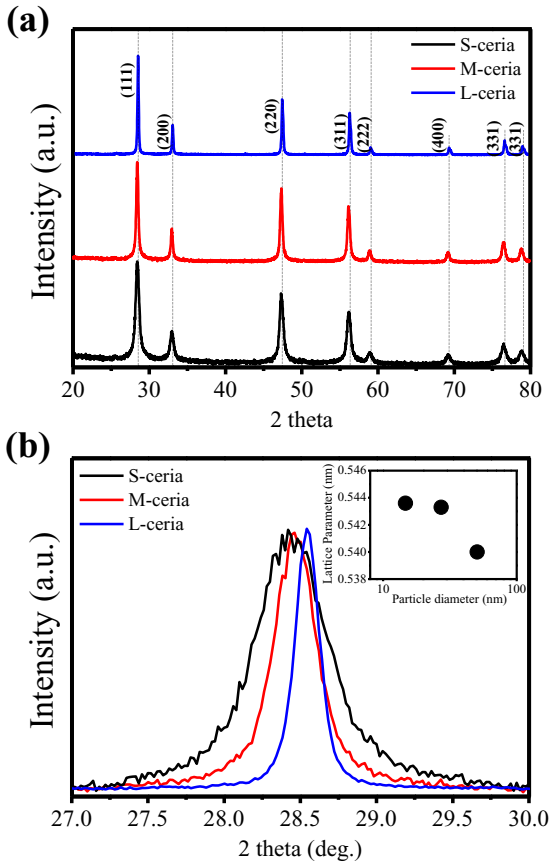

Figure 3. (a) XRD patterns of S-ceria, M-ceria, and L-ceria NPs. (b) Magnified images of the (111) peaks in XRD. The inset in (b) shows the lattice parameter of ceria NPs as a function of the particle diameter.

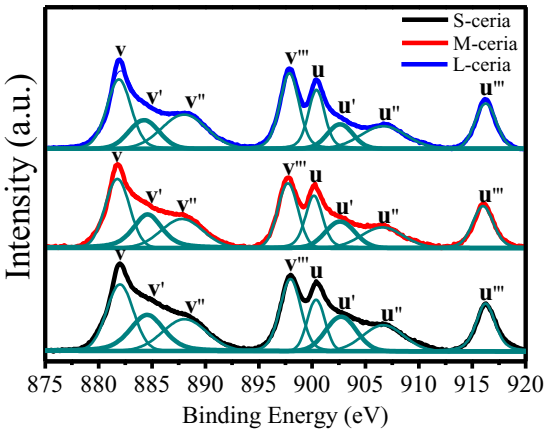

Figure 4. Ce 3d XPS spectra of S-ceria, M-ceria, and L-ceria NPs. The v' and u' peaks are characteristic of the Ce^{3+} ions.

110 nm (Figures 2a, 2b, and 2c). The average particle sizes of S-ceria, M-ceria, and L-ceria NPs were in the range of 60 to 80 nm. As shown in Figure 2g, the S-ceria NPs were composed of about 5 nm sized ceria primary NPs. The M-ceria NPs shown in Figures 2e and 2h were composed of primary ceria NPs that were about 30 nm in size. As shown in Figures 2f and 2i, the L-ceria NPs were single ceria NPs. Fast Fourier transformed (FFT) patterns of the S-ceria, M-ceria, and L-ceria NPs demonstrated their successful crystalline growth. HR-TEM analysis of all the ceria NPs revealed lattice fringes of 0.31, 0.27, and 0.18 nm that respectively corresponded to the (111), (002), and (220) planes of ceria NPs (Figures 2g, 2h, and 2i).[19,20] The clear (111), (002), and (220) lattice fringes of all the ceria NPs also indicated their successful crystalline growth. In addition, we also measured particle size distributions of S-ceria, M-ceria, and L-ceria NPs after dispersion in deionized water at pH 7 using DLS method to identify the dispersion stability of these ceria NPs. As shown in Figure S1, the average particle sizes of all the ceria NPs were about 170 nm. The larger size observed by DLS is due to the fact that the DLS measures the hydrodynamic diameters of the particle. This result indicated that all the ceria NPs were well dispersed in deionized water at pH 7.

Figure 3a shows the XRD patterns of S-ceria, M-ceria, and L-ceria NPs. The crystallite sizes (d_{XRD}) of all the ceria NPs were calculated from the full width at half maximum of the (111) peak by the Scherrer equation, and their lattice parameters were determined from the (111) diffraction peaks. The d_{XRD} values of S-ceria, M-ceria, and L-ceria were 14.7, 27.2, and 50.6 nm, respectively. Although the particle distributions of S-ceria, M-ceria, and L-ceria NPs were similar, the d_{XRD} values were different due to the differences in the size of their primary NPs. As shown in Figure 3b, the lattice parameters increased from 0.5400 to 0.5436 as the size of the ceria primary NPs decreased. The increase in lattice parameter was attributed to the increase in oxygen vacancy defects with increasing surface to volume ratio.[21,22] The oxygen vacancy defects leave behind two electrons located on two adjacent cerium ions, reducing their valence state from Ce^{4+} to Ce^{3+}.[23,24] In this regard, Ce^{3+} ions (1.143 Å), the radius of which is larger than that of Ce^{4+} ions (0.970 Å), leads to a lattice expansion of the cubic fluorite structure in ceria NPs.

XPS analysis was carried out to identify the differences in the oxidation states of S-ceria, M-ceria, and L-ceria NPs, which show different concentrations of Ce^{3+} ions on their surfaces. Figure 4 shows the Ce 3d XPS spectra for all the ceria NPs. To quantitatively calculate the concentration of Ce^{3+} ions, XPS spectra were deconvoluted into eight separate peaks using the Gaussian-Lorentzian function. The peaks for Ce 3d were split into the Ce $3d_{5/2}$ and Ce $3d_{3/2}$ ionizations. In the figure, peaks labeled v, v', v'', and v''' belong to the Ce $3d_{5/2}$ ionization, whereas the peaks u, u', u'', and u''' belong to the Ce $3d_{3/2}$ ionization.[15,25] Among these peaks, v' and u' are characteristic of Ce^{3+} ions, whereas v, v'', v''', u, u'', and u''' peaks are attributed to Ce^{4+} ions.[25] The concentrations of Ce^{3+} ions were calculated from the integrated area of the v and u peaks,[15] as follows.

$$[Ce^{3+}] = \frac{v' + u'}{v + v' + v'' + v''' + u + u' + u'' + u'''} \quad [1]$$

Table I provides details associated with the XPS analysis. As shown in Table I, the concentrations of Ce^{3+} ions in the S-ceria, M-ceria, and L-ceria were 24.0, 21.8, and 15.6%, respectively. These results showed that S-ceria NPs, having the smallest primary NPs, have the largest amount of Ce^{3+} at the surface. As particle size decreases, the large surface area to volume ratio results in an increase in Ce^{3+} concentration.[15] The decrease in particle size below 10 nm results in a remarkable increase of Ce^{3+} concentration.[17] M-ceria and S-ceria NPs have a larger Ce^{3+} concentration compared to L-ceria NPs. In addition, the S-ceria NPs, having about 5 nm sized ceria primary NPs, have the largest Ce^{3+} concentration. Although the particle sizes of all the ceria NPs were similar to each other, the different particle sizes of ceria primary NPs result in different concentrations of Ce^{3+} ions.

As we previously mentioned, the Ce^{3+} ions on the surface of ceria NPs play an important role as reactive sites. In CMP applications, Ce^{3+} groups react with hydrated silicate anions on the surface of a SiO_2 film, resulting in the formation of Ce–O–Si bonds.[7,11] Adsorption isotherms of silicate anions on S-ceria, M-ceria, and L-ceria NPs were plotted to elucidate the interactions between silicate anions and Ce^{3+} ions on the surface of ceria NPs. Figure 5 shows adsorption isotherms plotted for the adsorption of silicate anions onto the S-ceria, M-ceria, and L-ceria NPs at pH 7. The experimental data were analyzed using the Langmuir and Freundlich models.[26,27]

Table I. Ce 3d XPS peak assignments for S-ceria, M-ceria, and L-ceria NPs.

		Ce $3d_{5/2}$				Ce $3d_{3/2}$				
	Peak assignment	v Ce^{4+}	v′ Ce^{3+}	v″ Ce^{4+}	v‴ Ce^{4+}	u Ce^{4+}	u′ Ce^{3+}	u″ Ce^{4+}	u‴ Ce^{4+}	Ce^{3+} (%)
S-ceria	Binding energy (eV)	882	884.5	888.1	897.9	900.4	902.7	906.7	916.2	24.0
	Peak area (%)	17.4	13.8	13.5	15.7	8.7	10.2	10.1	10.6	
M-ceria	Binding energy (eV)	881.8	884.6	887.8	897.7	900.2	902.6	906.6	916	21.8
	Peak area (%)	18.8	13.2	13.3	14.5	11.4	8.6	9.5	10.7	
L-ceria	Binding energy (eV)	881.9	884.2	888.0	897.9	900.4	902.6	906.7	916.3	15.6
	Peak area (%)	18.9	9.0	16.1	17.0	11.6	6.6	10.8	10.0	

The Langmuir model can be expressed by the following equation:

$$\frac{C_e}{Q_m} + \frac{1}{bQ_m} = \frac{C_e}{Q_e}, \quad [2]$$

and the Freundlich model can be expressed by the following equation:

$$Q_e = K_F C_e^{\frac{1}{n}}, \quad [3]$$

where C_e (mg/L) is the equilibrium concentration of silicate anions in solution, Q_e (mg/m^2) is the amount of silicate anions adsorbed on the ceria NPs at equilibrium, Q_m is the maximum adsorbed amount (mg/m^2), and b is the Langmuir constant (L/mg).[26] The Freundlich constant K_F is related to the adsorption capacity, and 1/n is correlated with the adsorption intensity.[27]

Table II lists the constants calculated from the two models. The higher correlation coefficient (R^2) of the Freundlich model indicates that this model fits the data better than the Langmuir model. The Langmuir and Freundlich models assume the homogeneous and heterogeneous adsorption of silicate anions on the ceria NPs, respectively.[26,27] In this regard, it is reasonable to conclude that silicate anions were heterogeneously adsorbed on the surfaces of the ceria NPs as multilayers. In the case of S-ceria NPs, the amount of adsorbed silicate anions was 5.08 mg/m^2 at a silicate concentration of 1000 mg/L. In contrast, the values for M-ceria and L-ceria NPs were 3.96 and 2.28 mg/m^2, respectively. In addition, the value of K_F determined for S-ceria NPs was higher than those of the M-ceria and L-ceria NPs, indicating the higher adsorption capacity of the S-ceria NPs. This indicates that silicate adsorption with ceria NPs increased with increasing concentration of Ce^{3+} ions.

Table II. Langmuir and Freundlich constants for the adsorption of silicate ions on S-ceria, M-ceria, and L-ceria NPs.

	Langmuir constant			Freundlich constant		
	Q_m (mg/m^2)	b (L/mg)	R^2	K_F	1/n	R^2
S-ceria	16.4744	0.0007	0.8068	0.0125	0.8706	0.9867
M-ceria	11.5875	0.0006	0.8077	0.0104	0.8839	0.9808
L-ceria	7.2098	0.0005	0.7963	0.0062	0.8934	0.9897

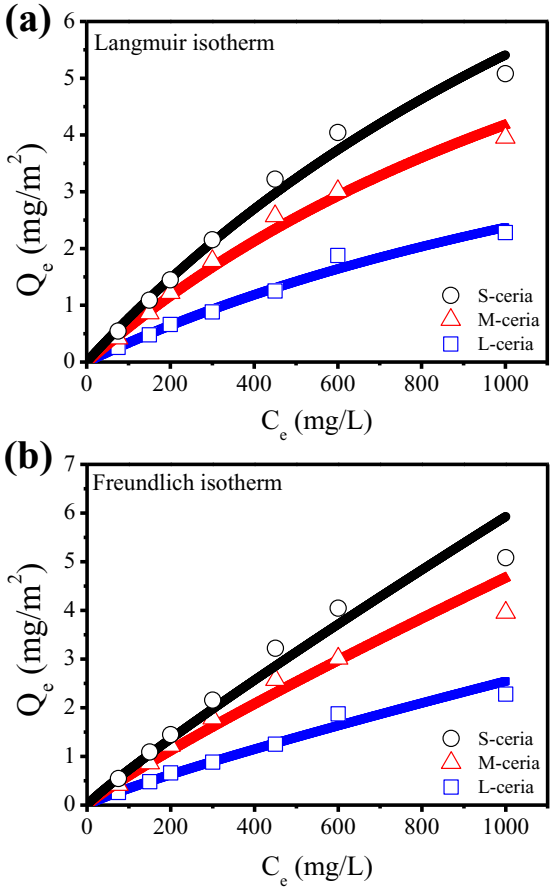

Figure 5. Adsorption isotherms of S-ceria, M-ceria, and L-ceria NPs as a function of silicate concentration at pH 7: (a) Langmuir and (b) Freundlich plots.

In CMP applications, ceria NPs are used as abrasives for the removal of SiO_2 films because they form Ce–O–Si bonds that help to remove SiO_2.[5,7,11] To identify the effects of SiO_2 removal with increasing Ce^{3+} ion content on the surface of ceria NPs, we applied S-ceria, M-ceria, and L-ceria NPs to the SiO_2 CMP process. As shown in Figure 6, the average removal rates of SiO_2 film using the slurries consisting of S-ceria, M-ceria, and L-ceria were 4301, 3890, and 3134 Å/min, respectively. These results corresponded well with the results of silicate adsorption. In the CMP process, both chemical and mechanical effects are highly related to the removal rate of SiO_2. In this regard, spherical shaped S-ceria NPs are at a disadvantage in terms

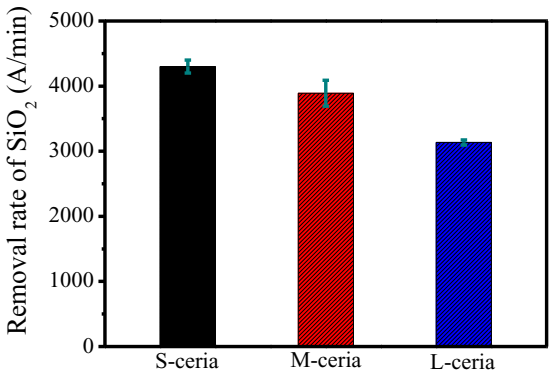

Figure 6. Removal rates of SiO_2 film by S-ceria, M-ceria, and L-ceria NPs at pH 7.

of the mechanical effects formed during the polishing process due to their low contact area with the wafer surface (see TEM images in Figure 2). However, the SiO_2 removal rate of S-ceria NPs was the highest compared to both M-ceria and L-ceria NPs. This result means that the chemical effect, related to the formation of Ce-O-Si, has more influence on the SiO_2 removal rate than mechanical effect. As a result, the high Ce^{3+} concentration of ceria NPs increased the chemical reaction with silicate anions, resulting in a high removal rate of SiO_2 during CMP. In addition, we applied S-ceria, M-ceria, and L-ceria NPs to the polishing of Si_3N_4 film because ceria NPs mainly applied to shallow trench isolation (STI) structure. As shown in Figure S2, the average removal rates of Si_3N_4 film using the slurries consisting of S-ceria, M-ceria, and L-ceria were 551, 509, and 485 Å/min, respectively. The removal selectivity of SiO_2 to Si_3N_4 of S-ceria, M-ceria, and L-ceria were 7.8, 7.6, and 6.4, respectively. This result is due to the fact that there are no additional additives for the high selectivity such as anionic surface or amino acid.[28,29] Furthermore, the surface properties such as nanotopography of SiO_2 and Si_3N_4 film after CMP are shown in Figure S3. The difference of the standard deviation (Rms) for the nanotopography in pre and post CMP was quite small.

Conclusions

We synthesized three different types of ceria NPs (S-ceria, M-ceria, and L-ceria NPs) to investigate the effect of Ce^{3+} concentration on the adsorption of silicate anions. As the particle size of the ceria primary NPs decreased from about 70 nm to 5 nm, the Ce^{3+} concentrations at the surface increased from 15.6 to 24.0%, respectively. The adsorption properties of S-ceria, M-ceria, and L-ceria with silicate anions were analyzed and fitted by both the Langmuir and Freundlich models. The adsorption isotherm was better fitted by the Freundlich model, which suggests a heterogeneous adsorption. The Freundlich constants (K_F and 1/n) indicated that the S-ceria NPs had a higher adsorption affinity for silicate anions than the M-ceria and L-ceria NPs. Finally, we applied all the ceria NPs to SiO_2 CMP. The results showed that the SiO_2 removal rate proportionally increased with increasing concentration of Ce^{3+} ions on the ceria surface.

Acknowledgments

This work was supported by the Korea Institute of Energy Technology Evaluation and Planning (KETEP) and the Ministry of Trade, Industry & Energy (MOTIE) of the Republic of Korea (No. 20168510050080).

References

1. H. Xiao, Z. Ai, and L. Zhang, *The Journal of Physical Chemistry C*, **113**, 16625 (2009).
2. T. Hibino, A. Hashimoto, T. Inoue, J.-i. Tokuno, S.-i. Yoshida, and M. Sano, *Science*, **288**, 2031 (2000).
3. A. I. Kozlov, D. H. Kim, A. Yezerets, P. Andersen, H. H. Kung, and M. C. Kung, *Journal of Catalysis*, **209**, 417 (2002).
4. T. Jiang, Z. Wang, J. Zhang, X. Hao, D. Rooney, Y. Liu, W. Sun, J. Qiao, and K. Sun, *J. Am. Ceram. Soc.*, **98**, 1717 (2015).
5. L. M. Cook, *Journal of Non-Crystalline Solids*, **120**, 152 (1990).
6. K. Kim, J. Seo, M. Lee, J. Moon, K. Lee, D. K. Yi, and U. Paik, *J. Mater. Res.*, 1 (2017).
7. J. Seo, J. Moon, J. H. Kim, K. Lee, J. Hwang, H. Yoon, D. K. Yi, and U. Paik, *Appl. Surf. Sci.*, **389**, 311 (2016).
8. M. J. Haron, F. Ab Rahim, A. H. Abdullah, M. Z. Hussein, and A. Kassim, *Materials Science and Engineering: B*, **149**, 204 (2008).
9. Z. Song, W. Liu, and H. Nishiguchi, *Catal. Commun.*, **8**, 725 (2007).
10. D. Marrocchelli and B. Yildiz, *The Journal of Physical Chemistry C*, **116**, 2411 (2012).
11. P. V. Dandu, B. Peethala, and S. Babu, *J. Electrochem. Soc.*, **157**, H869 (2010).
12. D. E. Vanpoucke, S. Cottenier, V. Van Speybroeck, I. Van Driessche, and P. Bultinck, *J. Am. Ceram. Soc.*, **97**, 258 (2014).
13. A. Bueno-López, K. Krishna, M. Makkee, and J. Moulijn, *J. Catal.*, **230**, 237 (2005).
14. T. Masui, K. Fujiwara, K.-i. Machida, G.-y. Adachi, T. Sakata, and H. Mori, *Chem. Mater.*, **9**, 2197 (1997).
15. S. Deshpande, S. Patil, S. V. Kuchibhatla, and S. Seal, *Appl. Phys. Lett.*, **87**, 133113 (2005).
16. S. Tsunekawa, K. Ishikawa, Z.-Q. Li, Y. Kawazoe, and A. Kasuya, *Phys. Rev. Lett.*, **85**, 3440 (2000).
17. R. Hailstone, A. DiFrancesco, J. Leong, T. Allston, and K. Reed, *The Journal of Physical Chemistry C*, **113**, 15155 (2009).
18. C. Zhou, L. Shan, J. R. Hight, S. Danyluk, S. Ng, and A. J. Paszkowski, *Tribology Transactions*, **45**, 232 (2002).
19. P. Huang, G. Chen, Z. Jiang, R. Jin, Y. Zhu, and Y. Sun, *Nanoscale*, **5**, 3668 (2013).
20. D. R. Ou, T. Mori, H. Togasaki, M. Takahashi, F. Ye, and J. Drennan, *Langmuir*, **27**, 3859 (2011).
21. L. Wu, H. Wiesmann, A. Moodenbaugh, R. Klie, Y. Zhu, D. Welch, and M. Suenaga, *PhRvB*, **69**, 125415 (2004).
22. S. Tsunekawa, R. Sivamohan, S. Ito, A. Kasuya, and T. Fukuda, *Nanostruct. Mater.*, **11**, 141 (1999).
23. P. Dutta, S. Pal, M. Seehra, Y. Shi, E. Eyring, and R. Ernst, *Chem. Mater.*, **18**, 5144 (2006).
24. N. Skorodumova, S. Simak, B. I. Lundqvist, I. Abrikosov, and B. Johansson, *Phys. Rev. Lett.*, **89**, 166601 (2002).
25. J. Shyu, W. Weber, and H. Gandhi, *The Journal of Physical Chemistry*, **92**, 4964 (1988).
26. I. Langmuir, *Journal of the American Chemical Society*, **38**, 2221 (1916).
27. H. Freundlich, *J. Phys. Chem*, **57**, 385 (1906).
28. S. K. Kim, S. Lee, U. Paik, T. Katoh, and J. G. Park, *J. Mater. Res.*, **18**, 2163 (2003).
29. P. W. Carter and T. P. Johns, *Electrochem. Solid-State Lett.*, **8**, G218 (2005).